Increasing output energy from a passively Q-switched Er:glass laser

Ronen Rabinovici, Amiel A. Ishaaya, Idit Peer, Liran Shimshi, Nir Davidson, and Asher A. Friesem

Department of Physics of Complex Systems, Weizmann Institute of Science, Rehovot 76100, Israel

*Corresponding author: ronen.rabinovici@weizmann.ac.il

Received 9 July 2007; revised 29 August 2007; accepted 31 August 2007;
posted 31 August 2007 (Doc. ID 85095); published 10 October 2007

A method for increasing the output energy from newly developed passively Q-switched Er:glass eyesafe lasers is presented. The increase of energy is achieved by incorporating binary phase elements inside the laser cavities. Experimental results reveal that the output energies can be increased by more than a factor of two. Moreover, by manipulating the output phase with the binary phase elements, the peak energy density in the far field is increased by more than a factor of 4.5. © 2007 Optical Society of America

OCIS codes: 140.0140, 140.3070, 140.3500, 140.3538, 140.3540, 140.3570, 140.3580.

1. Introduction

Recent progress in the development of passive Q-switches for infrared [1–5] lasers, and specifically of cobalt-doped glass ceramic [6,7] saturable absorbers, enables the realization of efficient passively Q-switched Er:glass lasers, which have several attractive features. They emit light of an eyesafe lasing wavelength at 1540 nm, have relatively short pulse width (most commonly between 20 and 60 ns), and are robust and compact. As a result, they can be incorporated into many applications, such as laser designators, laser range finders, wind metrology, LIDARs, and communication [8–10]. Passive Q-switches have many advantages over active ones. These include low cost, compact size and weight, robustness, and high reliability in harsh environmental conditions. One challenge in using passive Q-switches is to overcome their tendencies to control mode selection and beam narrowing [11,12].

In general, a possible approach for controlling mode selection and increasing the beam diameter is to incorporate binary phase elements into the laser cavities, as was done with Nd:YAG and CO_2 lasers, for selecting a single high-order mode [13,14]. The phase element along with an appropriate intracavity aperture introduces high losses to the undesired modes and low losses to the desired mode. Such phase elements were incorporated into a passively Q-switched Nd:YAG laser to select a TEM_{44} transverse mode to obtain output energy five-fold greater than when operating with TEM_{00} mode [15]. Such an approach with the intracavity binary phase elements is more difficult to implement with Er:glass lasers, since introducing a loss element into the cavity of such a laser can more easily eliminate laser operation. This is due to the fact that unlike the four-level gain medium of the Nd:YAG lasers, the Er:glass laser has three levels. Consequently, the single-pass gain of the Er:glass is approximately 2 orders of magnitude lower. Accordingly, when Er:glass lasers are passively Q-switched, only the lowest spatial mode can develop. Attempts to increase the pump power in order to increase the gain, unfortunately results in multipulsing behavior, which is unsuitable for many applications [16]. Thus, for most applications, with the saturable absorber passive Q-switch, the Er:glass lasers must be forced to operate at the lowest transverse Gaussian mode [17]. In this lowest transverse mode the volume of the gain medium is not fully exploited and therefore the output energies obtained are relatively low [18].

In this paper, we investigate and demonstrate how, despite the difficulties, it is possible to increase the output energy and to improve the stability and output beam quality of passively Q-switched Er:glass eyesafe lasers by inserting a binary phase element

0003-6935/07/307426-06$15.00/0

inside the cavity of the lasers. With the combination of the binary phase element and the saturable absorber passive Q-switch, the lasers operate at a preselected single high-order transverse mode so the volume of the gain medium is exploited more fully and thereby the output energy is increased. Stable lasing is obtained with such a combination. Moreover, it is possible to manipulate the phase of the selected mode so the light emerging from the laser has uniform phase, thereby resulting in a bright and focused spot with increased energy density in the far field.

2. Experimental Configuration

The experimental configuration is shown in Fig. 1. It includes an ~9 cm long basic laser resonator consisting of an Er:glass rod, of 2.2 mm diameter and 35 mm length, a highly reflective concave rear mirror, and a flat output coupler with ~85% reflectivity. The rod in our system is pumped with a flashlamp at a low pulse rate between 0.15 Hz and 0.25 Hz so as to ensure that it does not overheat. Higher rates are possible for the Er:glass lasers if cooling or diode pumping is exploited [17].

In addition, the configuration includes a saturable absorber passive Q-switch (SA PQS), a binary phase element (BPE) for selecting a desired transverse mode, and an adjustable aperture for ensuring that modes higher than that desired suffer from high losses to prevent them from lasing. In our experiments, the SA PQS was a 0.5 mm thick cobalt-doped transparent glass ceramic with antireflective layers on both sides. A 1.36 mm aperture was used for selecting the basic Gaussian TEM_{00} transverse mode. Three different BPEs, each with a corresponding aperture of 1.46, 1.86, and 2.2 mm, were used for selecting either TEM_{01}, TEM_{02}, or TEM_{04} degenerate Laguerre–Gaussian transverse modes, respectively. The BPEs were formed by ion etching several sectors on glass. The number of sectors corresponded to the transverse mode that was selected (i.e., two sectors for TEM_{01}, four sectors for TEM_{02}, and eight sectors for TEM_{04}; see Fig. 2). The thickness difference between adjacent sectors corresponds to a π-phase shift at the laser wavelength, and determined in accordance with $d = \lambda/2(n - 1)$, where n is the refractive index of the substrate. The substrates were then coated with antireflection layers in order to minimize undesired Fresnel reflections.

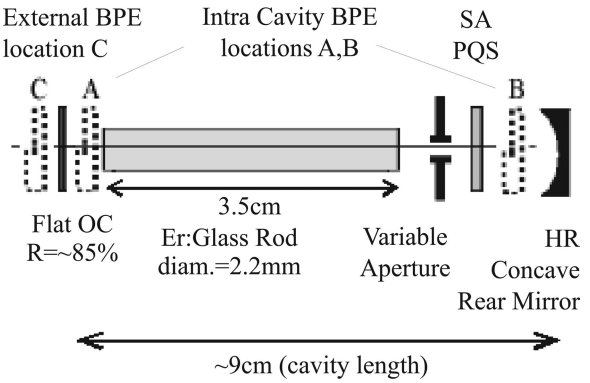

Fig. 1. Experimental configuration with two optional locations of the intracavity binary phase elements. The intracavity binary phase element can be either placed at position A—near the output coupler, or at position B—near the rear mirror. If positioned at A, the emitted light will have a uniform phase. If positioned at B, a second binary phase element should be placed at the exit from the output coupler, at position C, to obtain the uniform phase.

In some of our experiments the selected intracavity BPE was placed near the output coupler, denoted as location A in Fig. 1, so the phase of the emerging light was uniform, i.e., all lobes in the output transverse distribution had the same phase. Thus, the far-field intensity distribution would form a bright focused spot. In other experiments the intracavity BPE was placed near the rear mirror, denoted as location B in Fig. 1, so each lobe in the output transverse distribution had a π-phase shift from its adjacent lobes. Thus, the far-field intensity distribution would be similar to the near-field intensity distribution. When the intracavity BPE was placed at location B, another BPE, which is identical both in form and orientation, was placed immediately outside the laser, denoted as location C in Fig. 1. Thus, the light transmitted through the BPE at location C has a uniform transverse phase, so the far-field intensity distribution would again form a bright focused spot.

We detected the near- and far-field intensity distributions by means of two infrared vidicon cameras, and measured the corresponding laser output energies by means of a pyroelectric detector. The near-field intensity distributions were obtained by imaging the light distributions emerging directly from the laser (or when relevant, directly after passing through the external BPE) onto the infrared camera. The far-field intensity distributions were obtained after focusing the emerging light with a Fourier transform lens of 47 cm focal length onto the other camera.

3. Experimental and Calculated Results

The experimental and calculated results are presented in Figs. 2–5 and Table 1. Figure 2 shows experimental near-field and far-field intensity distributions with different BPEs. In the experiments the BPEs for selecting the TEM_{01}, and TEM_{02} modes were placed near the rear mirror so an external identical BPE was also used to obtain uniform transverse output phase and a bright focused far-field spot. The BPE for selecting the TEM_{04} mode was placed near the output coupler. There was no need to add an external BPE in order to obtain the uniform transverse output phase and a bright focused far-field spot. The corresponding measured energies were 4.01 mJ for TEM_{00}, 4.59 mJ for TEM_{01}, 6.34 mJ for TEM_{02}, and 8.78 mJ for TEM_{04}.

For comparison, we also show in Fig. 2 the calculated near-field and far-field intensity distributions for the different transverse modes with and without uniform phases. The near-field distribution for a regular pure degenerate Laguerre–Gaussian TEM_{pl} mode [14] is

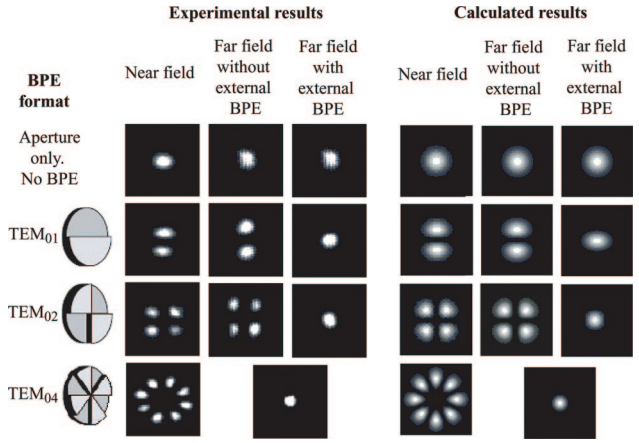

Fig. 2. (Color online) Experimental and calculated near-field and far-field intensity distributions with different BPEs. The BPEs for selecting the TEM_{01}, and TEM_{02} modes were placed near the rear mirror so an external identical BPE was also used to obtain uniform transverse output phase and a bright focused far field spot. The BPE for selecting the TEM_{04} mode was placed near the output coupler. As evident, there was no need to add an external BPE in order to obtain the bright focused spot with that arrangement.

$$E_{pl}(r,\ \theta) = E_0 \varrho^{l/2} L_p^{\ l}(\varrho) e^{-\varrho/2} \cos(l\theta), \tag{1}$$

where $\varrho = 2r^2/w^2$ with w as the spot size of the Gaussian beam, and $L_p^{\ l}$ are the generalized Laguerre polinomials of order p and index l. The near-field distribution for the mode with transversal uniform phase is

$$E(r,\ \theta)_{pl}|_{\text{uniform–phase}} = |E_{pl}(r,\ \theta)|. \tag{2}$$

The near-field intensity distributions, for the modes with and without uniform phases, are of course the same. The corresponding far-field intensity distributions were calculated from the far-field distributions that are obtained by Fourier transforming the near-field distributions of Eqs. (1) and (2). As evident, the calculated results are in good agreement with the experimental results. They indicate that the combination of an intracavity BPE with a SA PQS and an appropriate aperture indeed select a pure high-order Laguerre–Gaussian mode in the Er:glass laser.

It should be noted that the far-field energy distributions for the high modes with uniform phase should also contain side lobes [19]. They are not seen in Fig. 2 because their energy density is relatively low.

We developed a simple model for determining the output energies of TEM_{pl} modes emitted from a passively Q-switched laser. In this model we first assumed that the peak energies of the light falling on the PQS are the same for all the modes. Hence, the intracavity relative energies of the higher-order modes with respect to the fundamental Gaussian mode and to each other is readily obtained using Eq. (1). Specifically, the energy ratios between TEM_{00}, TEM_{01}, TEM_{02}, and TEM_{04} modes inside the cavity are 1:1.37:1.85:2.56, respectively. Next we assume that the diffraction losses of all the modes are the same, hence the output energy $U_{p,l}^{\ out}$ can be related to that of the internal energy $U_{p,l}^{\ in}$ [13] as

$$U_{p,l}^{\ out} = (1 - \gamma_d)(1 - \gamma_{OC}) U_{p,l}^{\ in}, \tag{3}$$

where γ_d are the diffraction losses and γ_{OC} are the output coupling losses. Accordingly, the ratios between the output energies of the modes should be the same as those inside the cavity.

To compare the model with the experimental results, we calculated the output energies of the TEM_{01}, TEM_{02}, and TEM_{04} modes using the measured output energy of the Gaussian TEM_{00} as 4.01 mJ. The calculated output energies were 5.49 mJ for TEM_{01}, 7.41 mJ for TEM_{02}, and 10.26 mJ for TEM_{04}. The corresponding measured output energies of 4.59 mJ, 6.34 mJ, and 8.78 mJ respectively, are 15% smaller than the results we obtained with this model. We believe that the discrepancies between the calculated and the experimental results are possibly due to additional losses introduced by the BPE, higher diffraction losses for the higher modes, and nonuniform gain distribution within the laser rod. The results of this model were also incorporated in all of the calculated results presented in this paper.

Figure 3 shows the experimental and calculated cross sections of the far-field energy distributions for

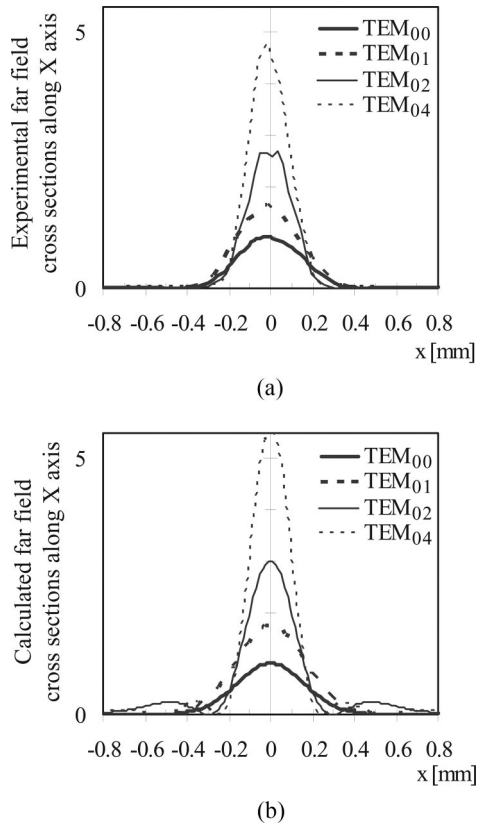

Fig. 3. Experimental and calculated cross sections of the far-field energy distributions for the four different modes with uniform phases. (a) Experimental; and (b) calculated.

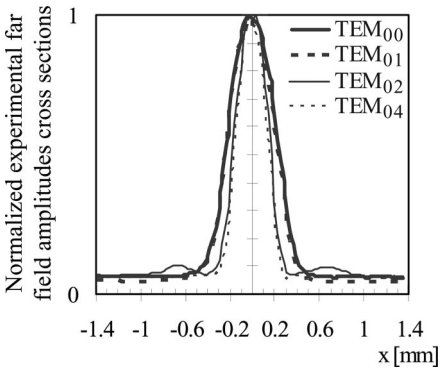

Fig. 4. Experimental cross sections of the far-field amplitude distributions for the four different modes with uniform phases.

the four different modes with uniform phases. As evident, the peak energy increases and the spot diameter decreases with the higher-order modes. We discovered that the experimental ratios of the energy peaks are 1:1.6:2.7:4.8 for the modes TEM_{00}, TEM_{01}, TEM_{02}, and TEM_{04}, respectively, while the corresponding calculated ratios are 1:1.7:3.0:5.5.

As is evident, the expected side lobes are clearly seen in the calculated results [Fig. 3(b)], but not in the experimental results [Fig. 3(a)]. Nevertheless, we also obtained side lobes experimentally when considering the normalized far-field amplitude distributions, as shown in Fig. 4, yet even these side lobes are lower than expected. In general, we attribute the reduction of the experimental side lobes to the low dynamic range and properties of our infrared vidicon camera.

Using the experimental and calculated far-field intensity distributions of the modes with uniform phases, shown in Fig. 2, and the corresponding experimentally measured and calculated total output energies, we determined how much energy falls within a virtual aperture of a certain diameter located at the far field. This allows us to exploit the energy-in-the-bucket (or the equivalent power-in-the-bucket) criterion, which is more relevant and useful when using binary phase elements, rather than the M^2 criterion [20,21]. The results are presented in Fig. 5. Figure 5(a) shows the experimental normalized relative energies of the four different modes as a function of the aperture diameter in the far field, and Fig. 5(c) the actual experimental energies of the four modes as a function of the aperture diameter in the far field, i.e., the experimental far-field energy-in-the-

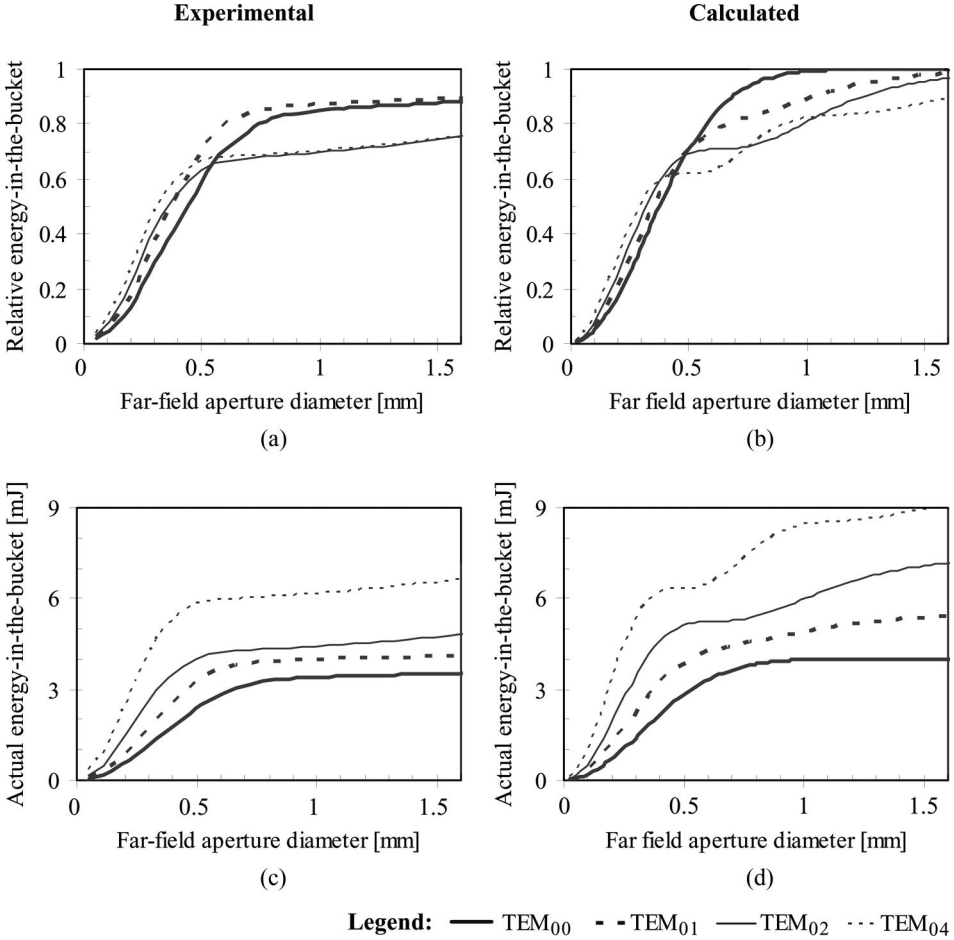

Fig. 5. Experimental and calculated energy in the bucket as a function of aperture diameter in the far field. (a) Experimental relative energies; (b) calculated relative energies; (c) experimental actual energies; and (d) calculated actual energies.

Table 1. Ratios Summary of Experimental and Calculated Output Energies Parameters

	TEM_{00}	TEM_{01}	TEM_{02}	TEM_{04}
Experimental output energy	1	1.14	1.6	2.19
Calculated output energy	1	1.37	1.85	2.56
Experimental peak energy at far field	1	1.6	2.7	4.8
Calculated peak energy at far field	1	1.7	3	5.5
Experimental far field central lobe width	1	0.87	0.67	0.61
Calculated far field central lobe width	1	0.82	0.64	0.53
Calculated percentage of energy in central lobe	100	85	71	62

bucket curves. Figures 5(b) and 5(d) show the corresponding calculated results, using a two-dimensional format.

In general, there is good agreement between the experimental and calculated results, for aperture diameters smaller than the main lobe width. Differences become evident for aperture diameters larger than the main lobe width. These differences are attributed again to the limiting properties of the infrared vidicon camera, which cannot detect the details of the side lobes. The background noise also becomes more dominant as the radius of integration increases. This is due to a reduction of the energy of the signal (i.e., signal-to-noise ratio is lower) and an increase in the area of integration. As is evident from the results of Figs. 5(c) and 5(d), it is better to operate the laser at the highest-order mode, where the output energies are highest and the divergence of the main lobe is lowest.

Table 1 summarizes the experimental and calculated results for several parameters of the output energies of the different modes with uniform phases. The results for each parameter are given in a relative form, with respect to the corresponding results of the fundamental TEM_{00} Gaussian mode. These results show that the output energy for the TEM_{04} is greater than a factor of two as compared with that of the TEM_{00} mode. Also, in the far field, the peak energy of the TEM_{04} mode is greater than a factor of 4.5 as compared with that of the TEM_{00} mode, and the diameter of the central lobe decreases by a factor of 1.6. The width of the central lobe for each operating mode was found as the average width at $1/e^2$ intensity points along far-field x and y axes. The percentage of energy contained in the central lobe for each mode was determined by the first inflection point in the corresponding energy-in-the-bucket curves shown in Fig. 5.

Finally, we performed some experiments to demonstrate that a BPE is indeed needed to obtain stable, high-energy output from passively Q-switched Er:glass lasers. Specifically, when we operated the laser without BPE, and increased the diameter of the aperture above 1.36 mm so as to obtain higher energy per pulse, we observed hot spots that were unstable both energetically and spatially.

4. Conclusion

To conclude, we have investigated and experimentally demonstrated the efficient selection of a single pure high-order transverse mode, in eyesafe passively Q-switched Er:glass laser configurations, overcoming the inherent spatial and temporal instabilities of these types of lasers. By incorporating phase elements into the cavity, the output energies were increased by more than a factor of two and the peak energy density in the far field was increased by more than a factor of 4.5. As a result the passively Q-switched Er:glass eyesafe lasers can be incorporated into a greater variety of applications.

We acknowledge support from M. Sirota, D. Abramovich, and I. Vilenchik, from Elbit Systems Electro-Optics ELOP Ltd.

References

1. M. Brumer, M. Sirota, A. Kigel, A. Sashchiuk, E. Galun, Z. Burshtein, and E. Lifshitz, "Nanocrystals of PbSe core, PbSe/PbS, and PbSe/$PbSe_xS_{1-x}$ core/shell as saturable absorbers in passively Q-switched near-infrared lasers," Appl. Opt. **45,** 7488–7497 (2006).
2. M. Birnbaum, M. B. Camargo, S. Lee, and F. Unlu, "Co^{2+}ZnSe saturable absorber Q-switch for the 1.54 μm Er^{3+}:Yb^{3+}:Glass laser," OSA TOPS **10,** 148–151 (1997).
3. R. D. Stultz, M. B. Camargo, and M. Birnbaum, "Passive Q-switch at 1.54 μm using divalent uranium ions in calcium flouride," J. Appl. Phys. **78,** 2959–2961 (1995).
4. M. B. Camargo, R. D. Stultz, M. Birnbaum, and M. Kokta, "Co^{2+}YSGG saturable absorber Q switch for infrared erbium lasers," Opt. Lett. **20,** 339–341 (1995).
5. R. D. Stultz, M. B. Camargo, and M. Birnbaum, "Q switch saturable absorber materials for solid state lasers," Proc. SPIE **2115,** 31–37 (1994).
6. Y. V. Volk, A. M. Malyarevich, K. V. Yumashev, O. S. Dymshits, A. V. Shashkin, A. A. Zhilin, U. Kang, and K. H. Lee, "Influence of reducing-oxidizing conditions on the optical properties of Co^{2+}-doped magnesium aluminosilicate glass ceramics and their use as an effective saturable absorber Q-switch," Appl. Opt. **43,** 6011–6015 (2004).
7. A. M. Malyarevich, I. A. Denisov, K. V. Yumashev, O. S. Dymshits, A. A. Zhilin, and U. Kang, "Cobalt-doped glass ceramic as a saturable absorber Q-switch for erbium:glass lasers," Appl. Opt. **40,** 4322–4325 (2001).
8. V. V. Akulinichev, I. V. Kurnin, and E. G. Kurochkina, "Eyesafe lidar by the solid state Er:glass laser," Proc. SPIE **5478,** 291–297 (2004).
9. R. Wu, M. J. Myers, J. D. Myers, and S. J. Hamlin, "Miniature and high repetition rate eyesafe Q-switched Er:glass transmitter for radar applications," Proc. SPIE **2748,** 378–384 (1996).
10. M. Sirota, E. Galun, V. Krupkin, A. Glushko, A. Kigel, M. Brumer, A. Sashchiuk, L. Amirav, and E. Lifshitz, "IV-VI semiconductor nanocrystals for passive Q-switch in IR," Proc. SPIE **5510,** 9–16 (2004).
11. W. R. Sooy, "The natural selection of modes in a passively Q-switched laser," Appl. Phys. Lett. **7,** 36–37 (1965).
12. A. Chandonnet, M. Piche, and N. McCarthy, "Beam narrowing by saturable absorber in a Nd:YAG laser," Opt. Commun. **75,** 123–128 (1990).

13. A. A. Ishaaya, N. Davidson, G. Machavariani, E. Hasman, and A. A. Friesem, "Efficient selection of high order Laguerre Gaussian modes," IEEE J. Quantum Electron. **39,** 74–82 (2003).
14. R. Oron, Y. Danziger, N. Davidson, A. A. Friesem, and E. Hasman, "Discontinuous phase elements for transverse mode selection," Appl. Phys. Lett. **74,** 1373 (1999).
15. A. A. Ishaaya, N. Davidson, and A. A. Friesem, "Very high order pure Laguerre Gaussian mode selection in a passively Q-switched Nd:YAG," Opt. Express **13,** 4952–4962 (2005).
16. R. Wu, T. Chen, J. D. Myers, M. J. Myers, and C. R. Hardy, "Multi-pulses behavior in a erbium glass laser Q-Switched by cobalt spinal," Proc. SPIE **5086,** 140 (2003).
17. R. Wu, S. J. Hamlin, J. A. Hutchinson, and L. T. Marshall, "Laser diode pumped, passively Q-Switched Erbium:glass lasers," OSA TOPS **10,** 145–147 (1997).
18. A. E. Siegman, *Lasers* (University Science Books, 1986).
19. A. E. Siegman, "Binary phase plates cannot improve laser beam quality," Opt. Lett. **18,** 675–677 (1993).
20. A. E. Siegman, G. Nemes, and J. Serna, "How to (maybe) measure laser beam quality," OSA TOPS **17,** 184–199 (1998).
21. R. Oron, N. Davidson, and A. A. Friesem, "Continuous phase elements can improve laser beam quality," Opt. Lett. **25,** 939–941 (2000).